Article published in:

Proc. SPIE 9708, Photons Plus Ultrasound: Imaging and Sensing 2016, 97083G (15 March 2016)

The publication is available at SPIE via

https://doi.org/10.1117/12.2209368

PROCEEDINGS OF SPIE

SPIEDigitalLibrary.org/conference-proceedings-of-spie

Freehand photoacoustic tomography for 3D angiography using local gradient information

Kirchner, Thomas, Wild, Esther, Maier-Hein, Klaus, Maier-Hein, Lena

Thomas Kirchner, Esther Wild, Klaus H. Maier-Hein, Lena Maier-Hein, "Freehand photoacoustic tomography for 3D angiography using local gradient information," Proc. SPIE 9708, Photons Plus Ultrasound: Imaging and Sensing 2016, 97083G (15 March 2016); doi: 10.1117/12.2209368

SPIE.

Event: SPIE BiOS, 2016, San Francisco, California, United States

Freehand photoacoustic tomography for 3D angiography using local gradient information

Thomas Kirchner[a], Esther Wild[a], Klaus H. Maier-Hein[b], and Lena Maier-Hein[a]

[a]Computer-Assisted Interventions, German Cancer Research Center (DKFZ), Heidelberg, Germany
[b]Medical Image Computing, German Cancer Research Center (DKFZ), Heidelberg, Germany

ABSTRACT

Photoacoustic tomography (PAT) is capable of imaging optical absorption in depths beyond the diffusion limit. As blood is one of the main absorbers in tissue, one important application is the visualization of vasculature, which can provide important clues for diagnosing diseases like cancer. While the state-of-the-art work in photoacoustic 3D angiography has focused on computed tomography systems involving complex setups, we propose an approach based on optically tracking a freehand linear ultrasound probe that can be smoothly integrated into the clinical workflow. To this end, we present a method for calibration of a PAT system using an N-wire phantom specifically designed for PAT and show how to use local gradient information in the 3D reconstructed volume to significantly enhance the signal. According to experiments performed with a tissue mimicking intralipid phantom, the signal-to-noise ratio, contrast and contrast-to-noise ratio measured in the full field of view of the linear probe can be improved by factors of 1.7 ± 0.7, 14.6 ± 5.8 and 2.8 ± 1.2 respectively, when comparing the post envelope detection reconstructed 3D volume with the processed one. Qualitative validation performed in tissue mimicking gelatin phantoms further showed good agreement of the reconstructed vasculature with corresponding structures extracted from X-ray computed tomographies. As our method provides high contrast 3D images of the vasculature despite a low hardware complexity its potential for clinical application is high.

Keywords: Photoacoustic Tomography, Freehand, Vasculature, Vesselness, Calibration, Angiography, 3D Reconstruction, PAUS

1. INTRODUCTION

Photoacoustic tomography (PAT) is a versatile biomedical imaging modality utilizing illumination of tissue with short laser pulses, which where absorbed, give rise to ultrasonic waves. It is thereby capable of imaging optical absorption in depths beyond the diffusion limit. One application of PAT is the imaging of vasculature.[1] While photoacoustic (PA) imaging is ideally suited to image blood vessels with intrinsic hemoglobin contrast or to image lymph vessels with exogenous contrast agents, challenges in this context include (1) the 3D reconstruction of a PAT volume without complex hardware setups and (2) the detection and localization of vessels in the reconstructed volume despite noise and artifacts in the image. In this paper, we take first steps to address these issues by adapting methods originally introduced for ultrasound (US) image processing. Firstly, we present a concept for reconstructing 3D PAT data from 2D PAT slice images, which is based on optical tracking and hand-eye calibration of a freehand PAT probe. Secondly, we propose a method using local gradient information to enhance vessel-like structures in PAT volumes and validate its performance on tissue mimicking vasculature phantoms.

2. MATERIALS & METHODS

The materials part of this section describes the PAT system and the characteristics of the PA phantoms as well as instructions on how to create these phantoms. The second part focuses on the calibration of PAT systems, while experiments for qualitative and quantitative evaluation as well as for signal enhancement are presented in section 3.

Please address your correspondence to Thomas Kirchner, e-mail: t.kirchner@dkfz-heidelberg.de
or Lena Maier-Hein, e-mail: l.maier-hein@dkfz-heidelberg.de

Photons Plus Ultrasound: Imaging and Sensing 2016, edited by Alexander A. Oraevsky, Lihong V. Wang
Proc. of SPIE Vol. 9708, 97083G · © 2016 SPIE · CCC code: 1605-7422/16/$18 · doi: 10.1117/12.2209368

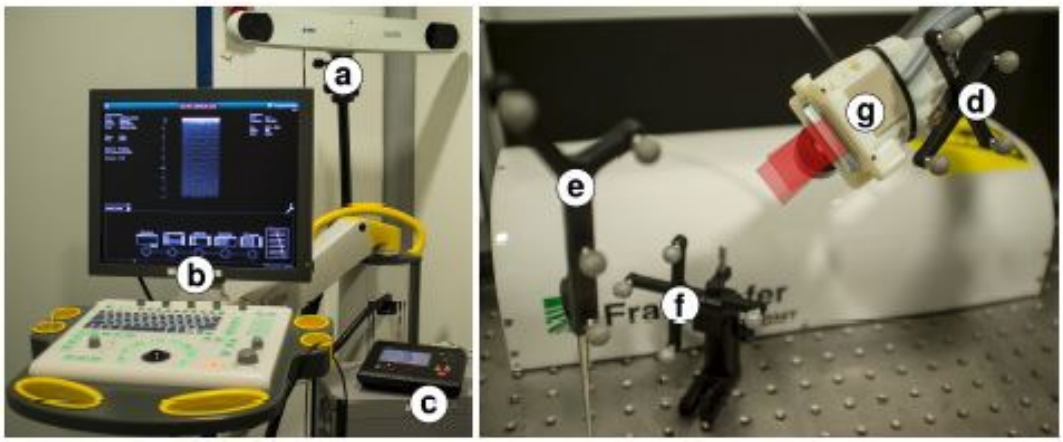

Figure 1. Tracked freehand PAT system: **(a)** Stereo camera for optical tracking, **(b)** control panel and interface for the US system and tracking, **(c)** laser control panel, **(d)** tracker mounted to the linear probe, **(e)** stylus used in phantom calibration, **(f)** reference marker used for phantom calibration, **(g)** PAT linear probe and mounted fiber bundles with indicated (red) laser output.

2.1 Materials

2.1.1 Setup

The freehand combined photoacoustic ultrasound (PAUS) system used for this work is a modified *DiPhAS* system (Fraunhofer IBMT, St. Ingbert, Germany, see fig. 1). A Nd:YAG laser operating at a wavelength of 1064 nm is used for PA signal generation. US imaging with the system is possible with a frame rate of up to 150 Hz, the PA imaging frame rate is limited to 20 Hz by the pulse repetition rate of the laser. The probe is a 128-element linear transducer with a 7.5 MHz center frequency and is tracked using an optical tracking system (*Polaris Spectra*, NDI Medical, Waterloo, Canada). For this purpose, a passive marker is attached to the linear probe; an additional reference marker mounted to the calibration phantom and a stylus are used for probe calibration as detailed in section 2.2.1.

The PAUS system is capable of live PA and US imaging. In addition to visualizing these image steams, radio frequency (rf) data is recorded for more involved off line data processing as described in sec 2.2.2. The Medical Imaging Interaction Toolkit (MITK)[*2] and its extension for image guided therapy MITK-IGT[3] in combination with the Public Software Library for Ultrasound Imaging Research (PLUS)[4] toolkit are used for that purpose.

2.1.2 Vasculature Mimicking Phantom

To assess the PAT system's capability to image vasculature, phantoms with realistic acoustic and optical properties for vasculature as well as the surrounding tissue are needed. For this purpose we use gelatine as a base material (following Cook *et. al.*[5]), which can yield these properties for US as well as PA imaging.

The phantom is prepared according to the following procedure: An acrylic glass box (constructed by the research and development workshop of the German Cancer Research Center (DKFZ)) featuring grids with 5 mm spacing on two opposing sides (see figure 2 a and b) holds the phantoms. Silicon tubing of 1.8 mm outer and 1 mm inner diameter is arranged through boreholes in the grid to mimic vasculature. After arranging the tubing, the phantom box is filled either with a gelatine mixture or for initial tests only with an intralipid-water mixture. The tubing is arranged in such a way to allow the injection of india ink, as suggested by Pouge *et al.* as the only readily available chromophore with suitable absorption in near infrared (NIR).[6] India ink has an absorption coefficient of very approximately $4000\,\mathrm{cm}^{-1}$ at 1064 nm. For use in the phantoms, it is diluted incrementally until arriving at the desired absorption (i. e. fully oxygenated whole blood, $\mu_\mathrm{a}(1064\,\mathrm{nm}) \approx 4\,\mathrm{cm}^{-1}$), which is measured using a spectrometer (*HR2000+*, Ocean Optics, Inc., Dunedin, USA). The main issue with using heavily diluted india ink is its unstable nature – it is only emulsified in water and will clump in a matter of hours. Freshly diluted india ink should therefore be injected directly prior to experiments.

For the gelatine mixture, de-mineralized water mixed with $1\,\mathrm{g\,l}^{-1}$ of *formaldehyde* (37 % by weight) is heated to 30 °C using a heater with a magnetic stirrer. $80\,\mathrm{g\,l}^{-1}$ of granular *gelatine* is slowly added under permanent stirring, while starting to heat the mixture to 50 °C, where the temperature is then held constant for 45 min while the mixture is continuously

[*] http://mitk.org/

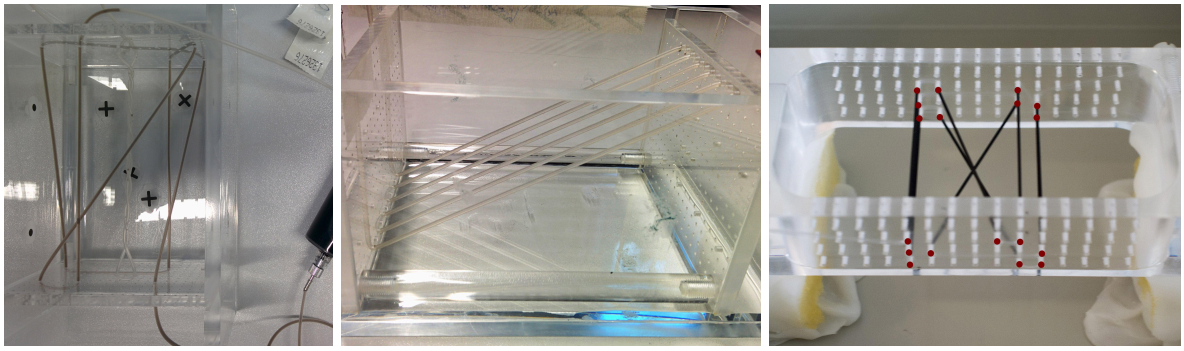

Figure 2. **(a)** Phantom holder with silicon tubing and diluted india ink as described in sec. 2.1.2. **(b)** Quantification phantom setup as described in the Vessel evaluation Experiment. **(c)** N-wire phantom modified for freehand PAT probe calibration as described in sec 2.2.1.

stirred at a rate slow enough that no new air bubbles are introduced. The mixture is then cooled to 40 °C before the addition of 50 g l^{-1} *intralipid* (20 % fat emulsion) (Santa Cruz Biotechnology, Inc. Dallas, Texas). Using the continuous magnetic stirring in concert with the low gelatin content through the use of formaldehyde eliminates air enclosures with simple means. After pouring the gelatine into any desired phantom form, phantoms are placed in cold-storage at 3 °C for a minimum of ten hours, to harden.

Phantoms produced in that way are very durable[6] (more than one week) if fresh ink is injected before every experiment. After initial cooling, they can endure higher temperatures without decay or deformation due to the cross linking formaldehyde. This is especially important for the PA signal intensity in phantoms due to the temperature dependent Grüneisen coefficient.[7]

2.2 Methods

For the volume reconstruction of PAT images, a synchronization and spatial calibration is necessary. Synchronization is necessary between tracking and imaging data for matching the correct position data to the recorded image slice. The spatial calibration is a prerequisite for volume reconstruction. The first part of this section describes the entire calibration process and the volume reconstruction (sec. 2.2.1), the second part (sec. 2.2.2) presents a method to enhance the contrast of vasculature.

2.2.1 Calibration and Volume Reconstruction

A temporal calibration or synchronization is necessary to account for delays in the data acquisition and processing of the probe and the recorded tracking data. To that end, we adapted a well-known technique for US synchronization,[8] where a probe is placed in a water tank and moved up-and-down in a sinusoidal fashion: For synchronization using the PA signal, a strongly absorbing, anodized aluminum foil is fixed to the bottom of the water tank to generate a PAT signal at the bottom.

For spatial calibration of the freehand PAUS system, we adapted a semi-automatic method with a modified triple layer N-wire phantom.[9] The phantom uses blackened nylon wiring, 0.6 mm in diameter, as shown in figure 2 c; the black coloring is neede to facilitate PA signal generation. The phantom is placed in a water tank and fixed to the tank by 2 cm blocks formed of a thermoplastic[†].

In an initial step, a stylus (fig. 1 e) is calibrated using the pivot algorithm of the PLUS toolkit. This stylus is then used for a point based registration to determine the pose of the reference tracker (fig. 1 f) relative to the coordinate system of the N-wire phantom, again using the PLUS toolkit(phantom registration). The tank holding the N-wire phantom is then filled with de-mineralized water of 5 cm depth. After ensuring that no air bubbles formed, 5 ml of intralipid 20 % is added to the water and mixed. This is done to homogenize light fluence at the edges of the imaging plane. The intralipid is another addition to adapt the US method for PAT imaging. The setup then rests half an hour for suspended dust particles to drop to the tanks bottom. During the final step, the actual spatial calibration of the probe, the PAUS probe is supported by a loose metal arm to facilitate a slow and steady motion whilst acquiring calibration data with a slow sweep over the N-wire phantom. The recorded image data is matched to the temporal nearest neighbor tracking data – taking the offset, ascertained by the synchronization, into account. The PLUS toolkit is then used to automatically perform the calibration.

[†]Polycaprolactone; useful for rapid prototyping due to its melting point of 60 °C

A pixel nearest neighbor (PNN) algorithm with *pixel trilinear interpolation*[10] implemented in PLUS is used for 3D reconstruction to receive volumetric imaging data. One main concern for the used 3D reconstruction algorithm is runtime for real-time imaging. The runtime for an algorithm has to be smaller than 50 ms per slice, to enable video frame rate imaging. PNN with pixel trilinear interpolation had been reported to take 50 ms per 320×240 pixels images on high end 2002 hardware,[10] while yielding high-quality results.[11] The time to add one slice to a reconstructed volume using the PLUS toolkit and the PNN algorithm only, has lately been reported to be 3 ms on 495×488 8-bit US image frames running on four threads on a more recent Intel Core i5-2520M laptop.[4] These algorithms should therefore be real-time capable, considering current hardware and our small image size of 303×200 pixels.

2.2.2 Vessel Enhancement

Imaging vasculature with PAT yields a high contrast due to the high optical absorption of blood, without the need for contrast agents. However, especially freehand PAT still suffers from a relatively high noise and some imaging artifacts. We therefore propose enhancing vessel contrast by analyzing local gradient information. For this purpose, we apply the so-called *Vesselness* filter, which has already successfully been applied for the enhancement of vasculature contrast in modalities such as X-ray computed tomography (CT).[12,13] In general, this method can be used to enhance curvilinear structures based on examining local gradient information. In an initial step, a Gaussian smoothing filter is applied to the image. This already reduces noise but more importantly tunes the responses of the Vesselness filter to an approximate radius defined by standard deviation σ of the Gaussian. This will result in a lowered response for vessels of different radius. For that reason, the filter is usually applied on multiple scales σ and the results are integrated. After the image is Gaussian-smoothed, the Hessian of it is taken. To generalize orientation, the Vesselness filter then takes the eigenvalues of the Hessian for every voxel – being $\lambda_1(\vec{x})$, $\lambda_2(\vec{x})$ and $\lambda_3(\vec{x})$, their notation order is defined by their magnitude ($\lambda_1(\vec{x}) \geq \lambda_2(\vec{x}) \geq \lambda_3(\vec{x})$). The eigenvector $\vec{e_1}$ corresponding to $\lambda_1(\vec{x})$ therefore defines the direction in which the second derivative is maximum, $\lambda_1(\vec{x})$ being the maximum second derivation value itself. The measure used for the Vesselness of a voxel is then $\lambda_c \cdot f$ with $\lambda_c = \min(-\lambda_2, -\lambda_3) = -\lambda_2$ and $f(\lambda_1, \lambda_c)$ which decreases with deviation of λ_1 from zero and uses λ_c for normalization.

$$f(\lambda_1, \lambda_c) = \begin{cases} \exp(-\frac{\lambda_1^2}{2(\alpha_1 \lambda_c)^2}) & \lambda_1 \leq 0, \lambda_c \neq 0 \\ \exp(-\frac{\lambda_1^2}{2(\alpha_2 \lambda_c)^2}) & \lambda_1 > 0, \lambda_c \neq 0 \\ 0 & \lambda_c = 0 \end{cases} \quad (1)$$

The parameters should obey $\alpha_1 < \alpha_2$. Following the recommendation by Sato *et. al.*,[12] we use $\alpha_1 = 0.5$ and $\alpha_2 = 2$, which have been found suitable for continuous enhancement of curvilinear structures while suppressing noise and other structures.

3. EXPERIMENTS

Three experiments were conducted to (1) assess the performance of our calibration method (sec. 2.2.1), (2) investigate qualitatively the reconstructed freehand PAUS volume and vessel enhancement and (3) evaluate the enhancement of vessels through the vesselness filter quantitatively.

3.1 Calibration

To assess the performance of our calibration method, spatial calibrations were performed after synchronization, using the methods described in section 2.2.1. For the synchronization, system-time-stamped measurements were taken from the tracking system using MITK-IGT, tracking the PAT probe only. The tracking system was configured to track at 30 Hz while the PA images were recorded with 20 Hz or US images with approximately 80 Hz. The temporal evolution of the elevation detected in the images taken by the probe was compared to the evolution of the probe marker elevation. The temporal offset of the two sinusoidal signals were measured at every zero-crossing and averaged.

The stylus was calibrated using the 200 tracking data sets taken over 20 seconds of pivoting. This stylus was then used for an eight point based registration of the phantom to its reference tracker. The rf calibration data was acquired with six to ten second sweeps of the probe over the calibration phantom. Twelve such data acquisitions were performed under the same conditions, to establish calibration quality; six with PA data and six with US data.

B-mode images were formed from the acquired US rf data, including the typical logarithmic filter. This filter was omitted for the PA B-mode image formation, due to sufficient contrast. The N-wire segmentation and calibration of the PLUS toolkit was performed on all twelve data sets. The segmentation parameters for wire detection were optimized manually in the PLUS graphical user interface (GUI) at one US and one PA data set. The remaining respective five segmentations were performed using those same parameters. Using the calibrated system, the segmented wires of the

images were reprojected onto the registered phantom to estimate calibration error. The calibration quality was quantified using the reprojection error, which is the root-mean-squared distance of all segmented wires to their respective registered wires. The reprojection errors for each calibration were then averaged.

3.2 Volume Reconstruction

Three different volumes were acquired and reconstructed, to qualitatively investigate the freehand PAUS reconstructed volumes and PA vessel enhancement: The first volume served to illustrate the complementary value of PA and US on a straight forward example. The other two, qualitatively assessed the value of vesselness in PA volumes, with the last one being co-registered to a CT scan. The 3D reconstructions were performed using PNN with pixel trilinear interpolation and a voxel size of $0.5 \times 0.5 \times 0.5\,\mathrm{mm}$ in the reconstructed volumes.

Hybrid Imaging: First tests to assess the image quality of the 3D volumes reconstructed from freehand PAUS were performed on paper phantoms in water baths. An example of such paper phantoms is shown in figure 4 a. It was printed on $80\,\mathrm{g\,m^{-2}}$ office paper and placed 4 cm deep in a water bath, on top of a foam material to minimize acoustic reflection. About 20 ml condensed milk (20 % fat) was added as a scattering agent to approximate minimal scattering in tissue ($\mu_\mathrm{s} \approx 10\,\mathrm{cm^{-1}}$). A slow ($\approx 5\,\mathrm{s}$ for 50 mm) freehand data acquisition sweep over the paper phantom was performed perpendicular to the surface of the paper and in direction of reading. The 3D volume was reconstructed as described in section 2.2.1.

Enhanced Vessel Visualization: Two differently configured vasculature mimicking phantoms were constructed and imaged, both of them used silicon tubing with an inner diameter of 1 mm to simulate vasculature. Diluted ink (*Kunstschrift-Tusche*, Pelikan, Hannover, Germany) was injected into these vessels to simulate whole blood. The first vasculature phantom under investigation consisted of three parallel tubes, 5 mm apart at the depth of 3 cm. The structure was placed into a water-milk bath like the paper phantom, for a qualitative test of the Vesselness filter. A gelatine based phantom was constructed with the mixture described in sec 2.1.2 and a more complex tubing configuration, as shown in figure 2 a. The simulated vasculature was in a depth of 1 to 6.5 cm and filled with diluted ink with an absorption of $\mu_\mathrm{a}(1064\,\mathrm{nm}) = 4\,\mathrm{cm^{-1}}$.

PAT CT Fusion: In addition, eight small pieces of metal, painted black, were inserted into the gelatine phantom after it hardened to enable co-registration of the reconstructed PAT volumes and an additionally acquired high resolution CT scan.

PAT and tracking data were acquired with slow 8 s sweeps over the phantoms, using a water film on top of the gelatine phantom for optimal acoustic coupling.

3.3 Vesselness Evaluation

To quantify the enhancement of vasculature by the Vesselness filter, an additional vasculature mimicking phantom was specially designed to determine signal-to-noise ratio (SNR), contrast and contrast-to-noise ratio (CNR) at varying depths. The phantom vasculature consisted of eight parallel tubes, arranged with 5 mm spacing as an inclined plane and fixed on both sides of the phantom holder to depths of 0.5 mm and 7 mm respectively. A similar phantom can be seen in figure 2 b, before the box was filled with the gelatine mixture and the tubes injected with diluted ink. The data for 3D reconstructed PAT volume was acquired by a 10 s sweep along the tubes with the goal of imaging the tubes in depths of 1 cm to 5 cm. A metal arm was used to fix the elevation of the transducer. The Vesselness filter was applied to the reconstruction with $\sigma = 0.5\,\mathrm{mm}$.

Tubes directly visible in the PAT volume were detected manually in 21 parallel slices with original B-mode image orientation featuring tubes in depths of 11 mm to 34 mm. Automatic detection was very unreliable due to noise and artifacts close to the tubes. Signal intensity measurements for 129 tube intersection coordinates were manually measurable. The signal at the same coordinates in the Vesselness volume was also recorded. Values for the noise were acquired via the MITK statistics plugin by taking the average and standard deviation for the voxel intensities in large areas 5 mm below and above the signal, to exclude imaging artifacts.

The SNR, contrast and CNR of 3D freehand PAT volumes were investigated as image quality benchmarks. Those values can be defined as follows,[14]

$$\mathrm{SNR} = \frac{S}{\sigma(N)}, \quad \mathrm{contrast} = \frac{|S - \langle N\rangle|}{\langle N\rangle}, \quad \mathrm{CNR} = \frac{|S - \langle N\rangle|}{\sigma(N)} \tag{2}$$

with S being the signal intensity, $\langle N\rangle$ the average noise intensity and $\sigma(N)$ the standard deviation of the noise.

4. RESULTS

4.1 Calibration

The synchronization of tracking and image data, yielded a delay of 27 ms ± 8 ms (calculated from 22 zero-crossings). The calibration of the stylus had an error of 0.4 mm in stylus tip position, according to PLUS, the phantom registration yielded a 0.7 mm error. The deviations from the 3D reprojection errors for each of the twelve calibrations performed are consistently 0.2 ± 0.1 mm for both US and PAT and are plotted in figure 3.

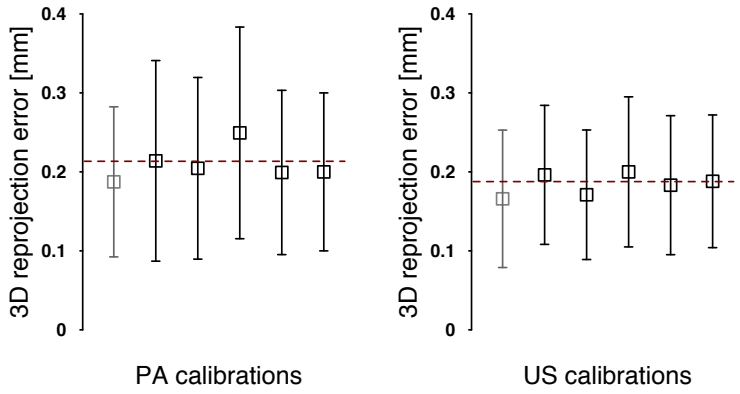

Figure 3. 3D reprojection errors with standard deviations as calculated by PLUS after calibration. The N-wire segmentation parameters were optimized for PA and US separately using the first (greyed out) data sets and then repeated five times for each modality.

4.2 Image and Volume Reconstruction

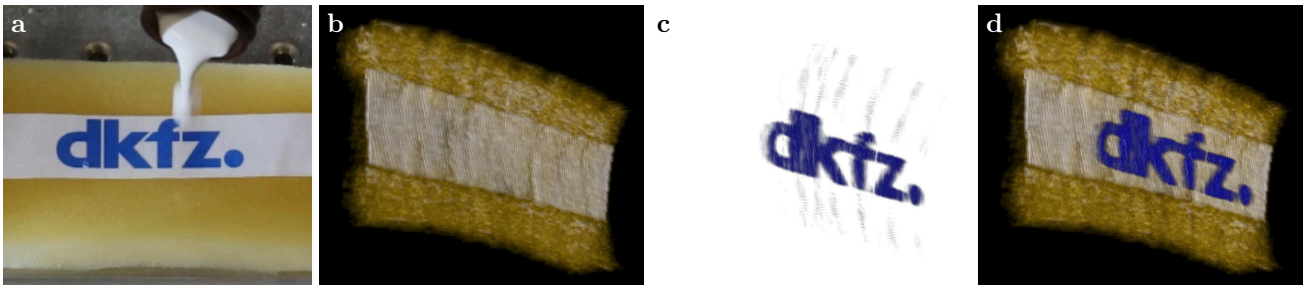

Figure 4. **(a)** The logo of the German Cancer Research Center printed on paper in a milk and water mixture. **(b)** The volume rendered 3D reconstruction of the US scan. **(c)** The volume rendered 3D reconstruction of the photoacoustic scan. **(d)** Superposition of the volume rendered 3D reconstructions.

On mid-size consumer hardware[‡], the processing time for 2D reconstruction per B-mode image was measured to be 27 ± 1 ms on $1024 \times 256 \times 16$ bit raw data images. Down-sampling the resulting B-mode image by a factor of three took an additional 9 ms. Adding one slice of $303 \times 200 \times 8$ bit size to the 3D volume took an average of 5 ms[§]. The reconstructed 3D volume of the paper phantom was volume rendered with MITK. The results can be seen in figure 4 b - d.

The volume renderings of the 3D reconstructed tubes can be seen in figure 5 a, alongside figure 5 b which shows the result of the Vesselness filter with $\sigma = 0.5$ mm. The measured spacing of the tubes in the reconstruction as well as their depth were consistent with the phantom.

[‡]2009, Intel Core i7 CPU 870
[§]here, using a Intel Core i7 3610-QE CPU

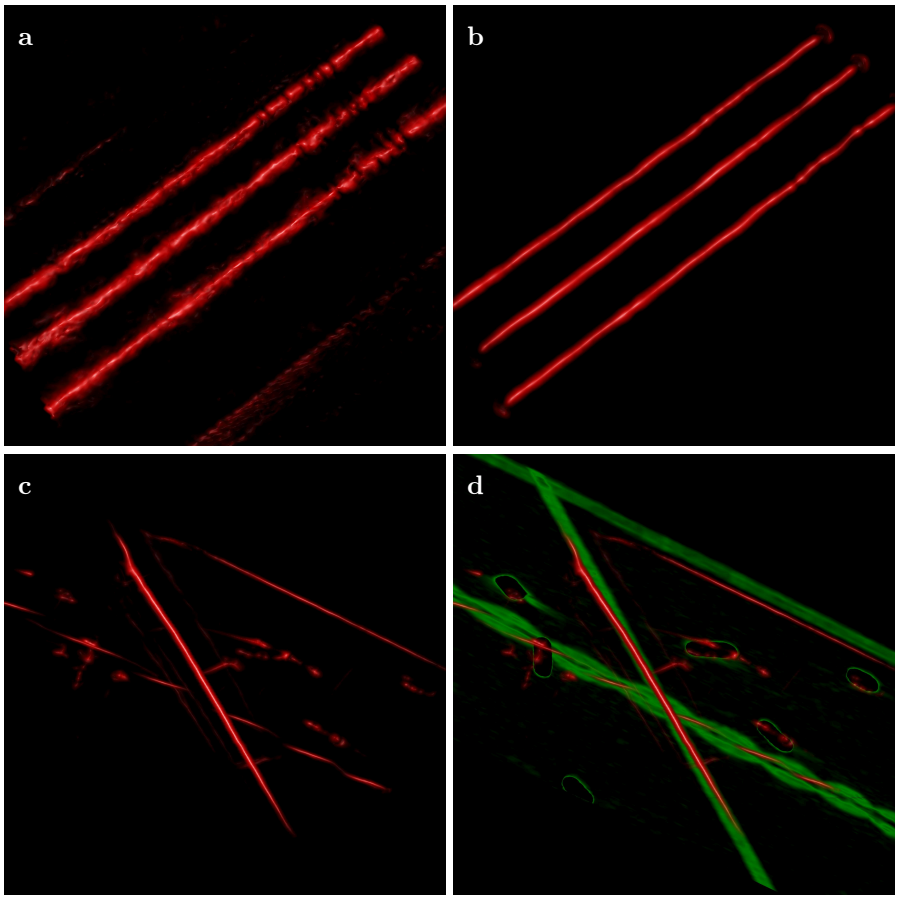

Figure 5. Vesselness comparison: Volume renderings of **(a)** a simple reconstructed vasculature phantom, **(b)** the Vesselness of volume (a), **(c)** the Vesselness of complex gelatine based phantom, **(d)** the manually rigid registered (c) in red to a CT volume in green. Small structures in (c) and (d) show metal wires used as landmarks for image registration.

The volume rendered result of the Vesselness filter on the PAT volume and the manual registration to the CT volume can be seen in figure 5 c and 5 d. The performed point based registration with eight manually set points on markers and landmark structures, yielded a registration error of 1.1 mm, only considering these eight points.

4.3 Vesselness Enhancement

SNR, contrast and CNR were calculated for each of the 2×129 positions. In figure 6, these values are plotted against their depth and lateral position in the original B-mode images, using a thin plate spline fit and a jet color map for visualization.

The vesselness enhancement factors SNR, contrast and CNR for 2×127 values are visualized with violin plots in figure 7 (two pairs of values were truncated because they resulted in a division by zero). Contrast was found to be enhanced by a factor of 14.6 ± 5.8. For SNR the enhancement factor was 1.7 ± 0.7, for CNR 2.8 ± 1.2.

5. DISCUSSION

In this paper, we presented a concept for 3D visualization of vascular structures using freehand 3D PAT. Our contribution is based on previously introduced methods for US image processing and comprises a method for 3D PAT reconstruction from 2D slices based on a tracked and calibrated PAT probe as well as a method for enhancing vasculature in PAT volumes. According to experiments in tissue mimicking phantoms, the proposed concept is well suited for freehand 3D PA angiography and yields an enhancement of contrast by an order of magnitude.

One of the main advantages of our approach is that it is based on a handheld device and can thus be smoothly integrated into the clinical workflow. Previous concepts were mainly based on complex hardware setups such as fixed

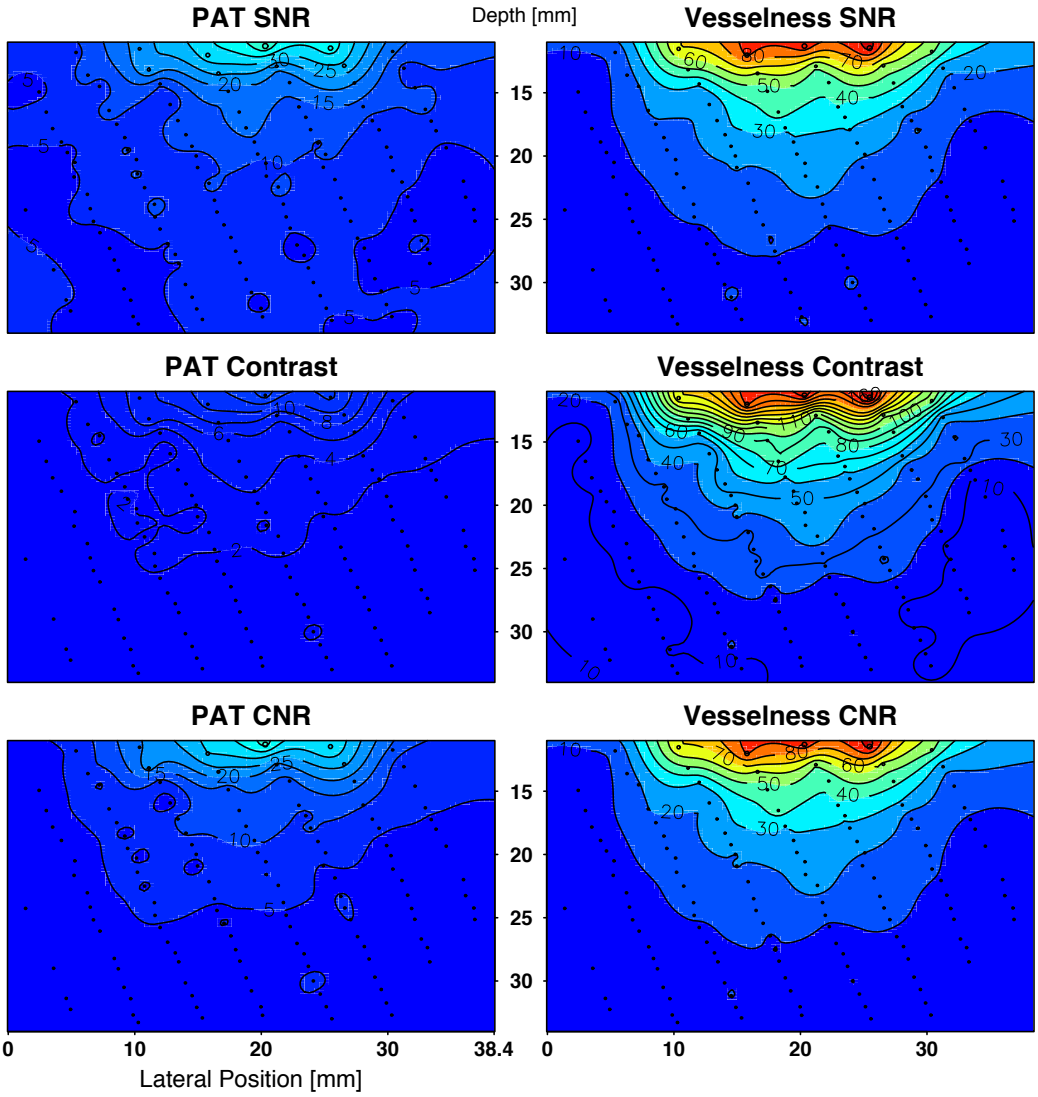

Figure 6. Spatial dependence of PAT image quality in terms of SNR, contrast and CNR for phantom vasculature before (left) and after (right) application of the Vesselness filter. The dots mark the measurements – interpolation was performed using a thin plate spline fit. This also visualizes the relative optical fluence in the image plane.

PA tomographs for mammographies.[15,16] Note that recent publications[17,18] have used freehand 3D reconstruction, but details on the methods were not provided or the methods are not real-time capable.[19]

The laser wavelength we used is not optimal for blood vessel imaging due to the comparably low absorption of blood at 1064 nm. While the use of tunable lasers is planned for future work, the current laser, which was chosen for its wide availability and simple handling, is sufficient for these initial tests. Another issue is the absorption of scattered laser light on the surface of the PAT probe in acoustic contact with the phantom or tissue. This is problematic because it yields a PA wave emanating from the probe, causing a weak conventional US image overlay with an offset to the PAT image. An attached reflective foil on top of the transducer minimized the artifact but the problem persists. A reflective coating over every part of the probe that comes in contact with the tissue should solve this problem.

Our system's synchronization of tracking and image data was relatively stable and the limited tracking frame rate was the main cause of fluctuations in the temporal offset. Synchronization should be integrated into an automatic calibration workflow, so that measurements can be easily taken prior to every experiment to account for varying system

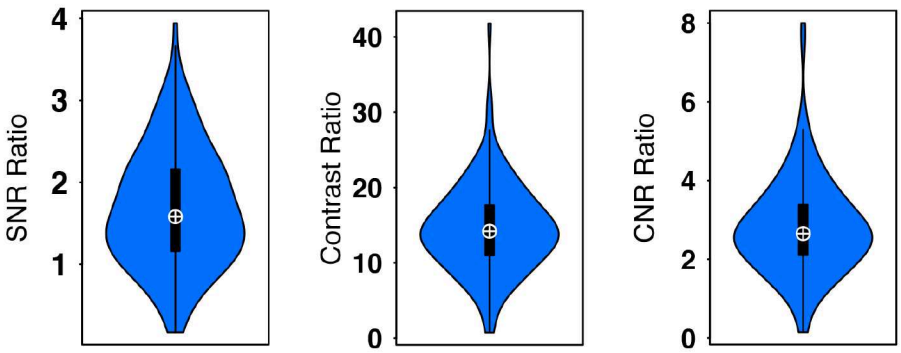

Figure 7. Vessel enhancement due to the Vesselness filter in terms of SNR, contrast and CNR. Violin plots showing the overall distribution of the ratios and boxplots with standard deviations.

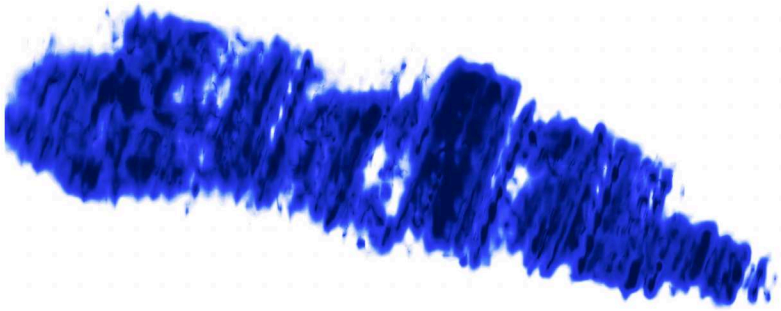

Figure 8. Volume rendering of the reconstruction results of a printed *dkfz.* logo, with fast, erratic freehand motion. (cf. steady reconstruction in figure 4 a and c)

configurations. It should be investigated further, how the synchronization varies with different tracking rates or with other changes in system configuration. Additionally, more sophisticated methods of matching the data streams might improve the synchronisation. The fluctuations in the temporal offset may be the cause for an additional problem; figure 8 shows an extreme example for rapid movement. Such rapid movement rather than slow sweeps over the region of interest can significantly distort the reconstructed volume.

The performed spatial calibrations, using the modified N-wire phantom, all yielded small reprojection errors (0.2 mm) considering that 0.5 mm usually implies an accurate calibration.[4] A look at the translational offset of the probe calibration results additionally yields a good agreement and a high precision of the PA and US calibrations among themselves. It should be noted that a systematic translational offset of approximately 1 mm exists between the spatial calibration of US and PA, which implies that it is advantageous to calibrate the two modalities separately.

The N-wire calibration procedure can be performed quickly and semi-automatically and yields high quality and highly reproducible results. The major disadvantage of N-wire calibration is the need for three separate calibration steps using different tracked markers, all of which yield tracking errors. Additional sub-millimeter deviations in the production of the phantom and unintentional shift during phantom registration are additional error sources. A direct point-based calibration of the probe, for example, eliminates one marker and one calibration step, including its intrinsic errors along with all phantom related errors. However, all calibration methods have different trade-offs in terms of calibration accuracy, speed, effort and dependence on the expertise of the user.[20]

Total reconstruction times for a single 2D B-mode image together with the runtime of the resampling of said image and writing the slice into a 3D volume were altogether lower then 50 ms, making it possible to perform those computing steps for video frame rates using MITK-US[21] and a laser with pulse repetition rate of 20 Hz. Furthermore, the largest part of the total reconstruction time with 27 ms for the B-mode image reconstruction can be improved further by computing on GPU instead of performing multi-threaded calculations on CPUs.

The co-registration of PAT volumes with CT images only showed an approximate qualitative agreement of the modalities. This was mainly due to the underwhelming visibility of the painted metal markers in PAT, probably caused by inadequate acoustic coupling of the markers, which were inserted in the already hardened gelatine. Registration could be

improved by inserting the marker during the cooling process of the gelatine and by better defined markers. First tests with graphite (pencil lead) looked promising, commercially available CT markers should work as well.

The quantification phantom experiment (sec. 3.3), in addition to providing a good validation for the vessel enhancement using the Vesselness filter on PAT volumes, also gives a good illustration of our system's effective laser fluence in the imaging plane. Contrast is enhanced most by the Vesselness filter. It should be noted that the assumption of a standard distributed noise, which is made implicitly by using standard deviation of noise, is not valid for Vesselness which has bimodal noise, caused by many zero-voxels. Even with that in mind, the enhancement of contrast is not dependent on this assumption and the SNR and CNR measures are still meaningful. In addition, all vessels in this paper were of the same size. The parameter $\sigma = 0.5\,\text{mm}$ was well chosen for this case but in more realistic settings, a multi scaled σ will be necessary, which will result in a reduction of contrast with respect to the reported value.

The Vesselness filter can be useful in a diagnostic or off line planning capacity, its interventional usefulness is limited to visualization after the acquisition of a full image volume due to its computing time in the order of ten seconds, using current high-end hardware.

In conclusion, the freehand PAT concept presented in this paper can be developed to be a potentially valuable diagnostic and interventional tool, providing enhanced contrast for angiography. Future work on a translational approach could also focus on the use of the method in lymph vessel visualization with exogenous PA contrast, as recent clinical studies have reported progress in that area.[17,18]

ACKNOWLEDGMENTS

The authors would like to acknowledge support from the European Union through the ERC starting grant COMBIOSCOPY under the New Horizon Framework Programme under grant agreement ERC-2015-StG-37960.

REFERENCES

[1] Deán-Ben, X. L. and Razansky, D., "Functional optoacoustic human angiography with handheld video rate three dimensional scanner," *Photoacoustics* **1**(3–4), 68–73 (2013).

[2] Nolden, M., Zelzer, S., Seitel, A., Wald, D., Müller, M., Franz, A. M., Maleike, D., Fangerau, M., Baumhauer, M., Maier-Hein, L., Maier-Hein, K. H., Meinzer, H. P., and Wolf, I., "The medical imaging interaction toolkit: challenges and advances," *International Journal of Computer Assisted Radiology and Surgery* **8**(4), 607–620 (2013).

[3] Franz, A. M., Seitel, A., Servatius, M., Zöllner, C., Gergel, I., Wegner, I., Neuhaus, J., Zelzer, S., Nolden, M., Gaa, J., Mercea, P., Yung, K., Sommer, C. M., Radeleff, B. A., Schlemmer, H.-P., Kauczor, H.-U., Meinzer, H.-P., and Maier-Hein, L., "Simplified development of image-guided therapy software with mitk-igt," in [*Proc. SPIE*], *Proc. SPIE* **8316**, 83162J–83162J–8 (2012).

[4] Lasso, A., Heffter, T., Rankin, A., Pinter, C., Ungi, T., and Fichtinger, G., "Plus: Open-source toolkit for ultrasound-guided intervention systems," *IEEE Transactions on Biomedical Engineering* **61**(10), 2527–2537 (2014).

[5] Cook, J. R., Bouchard, R. R., and Emelianov, S. Y., "Tissue-mimicking phantoms for photoacoustic and ultrasonic imaging," *Biomedical optics express* **2**(11), 3193 (2011).

[6] Pogue, B. W. and Patterson, M. S., "Review of tissue simulating phantoms for optical spectroscopy, imaging and dosimetry," *Journal of Biomedical Optics* **11**(4), 041102–041102–16 (2006).

[7] Wang, L. V. and Gao, L., "Photoacoustic microscopy and computed tomography: From bench to bedside," *Annual Review of Biomedical Engineering* **16**(1), 155–185 (2014). PMID: 24905877.

[8] Rousseau, F., Hellier, P., and Barillot, C., "Confhusius: A robust and fully automatic calibration method for 3d freehand ultrasound," *Medical Image Analysis* **9**(1), 25 – 38 (2005).

[9] Chen, T. K., Thurston, A. D., Ellis, R. E., and Abolmaesumi, P., "A real-time freehand ultrasound calibration system with automatic accuracy feedback and control," *Ultrasound in Medicine & Biology* **35**(1), 79 – 93 (2009).

[10] Gobbi, D. G. and Peters, T. M., "Interactive intra-operative 3d ultrasound reconstruction and visualization," in [*Medical Image Computing and Computer-Assisted Intervention — MICCAI 2002*], Dohi, T. and Kikinis, R., eds., *Lecture Notes in Computer Science* **2489**, 156–163, Springer Berlin Heidelberg (2002).

[11] Solberg, O. V., Lindseth, F., Bø, L. E., Muller, S., Bakeng, J. B. L., Tangen, G. A., and Hernes, T. A. N., "3d ultrasound reconstruction algorithms from analog and digital data," *Ultrasonics* **51**(4), 405–419 (2011).

[12] Sato, Y., Nakajima, S., Shiraga, N., Atsumi, H., Yoshida, S., Koller, T., Gerig, G., and Kikinis, R., "Three-dimensional multi-scale line filter for segmentation and visualization of curvilinear structures in medical images," *Medical Image Analysis* **2**(2), 143–168 (1998).

[13] Frangi, A., Niessen, W., Vincken, K., and Viergever, M., "Multiscale vessel enhancement filtering," in [*Medical Image Computing and Computer-Assisted Interventation — MICCAI'98*], Wells, W., Colchester, A., and Delp, S., eds., *Lecture Notes in Computer Science* **1496**, 130–137, Springer Berlin Heidelberg (1998).

[14] Kang, H.-J., Lediju Bell, M. A., Guo, X., Taylor, R. H., and Boctor, E. M., "Freehand spatial-angular compounding of photoacoustic images," in [*Photons Plus Ultrasound: Imaging and Sensing 2014*], *Proc. SPIE* **8943**, 894361–894361–9 (2014).
[15] Kruger, R., Reinecke, D., Del Rio, S., Lam, R., and Doyle, R., "Photoacoustic angiography of the breast," *Medical Physics* **37**(11), 6096–6100 (2010).
[16] Manohar, S., Vaartjes, S. E., van Hespen, J. C. G., Klaase, J. M., van den Engh, F. M., Steenbergen, W., and van Leeuwen, T. G., "Initial results of in vivo non-invasive cancer imaging in the human breast using near-infrared photoacoustics," *Optics Express* **15**(19), 12277–12285 (2007).
[17] Stoffels, I., Morscher, S., Helfrich, I., Hillen, U., Leyh, J., Burton, N. C., Sardella, T. C. P., Claussen, J., Poeppel, T. D., Bachmann, H. S., Roesch, A., Griewank, K., Schadendorf, D., Gunzer, M., and Klode, J., "Metastatic status of sentinel lymph nodes in melanoma determined noninvasively with multispectral optoacoustic imaging," *Science Translational Medicine* **7**(317), 317ra199–317ra199 (2015).
[18] Garcia-Uribe, A., Erpelding, T. N., Krumholz, A., Ke, H., Maslov, K., Appleton, C., Margenthaler, J. A., and Wang, L. V., "Dual-modality photoacoustic and ultrasound imaging system for noninvasive sentinel lymph node detection in patients with breast cancer," *Scientific Reports* **5**, 15748 (2015).
[19] Li, G., Xia, J., Li, L., Wang, L., and Wang, L. V., "Isotropic-resolution linear-array-based photoacoustic computed tomography through inverse radon transform," in [*Proc. SPIE*], *Proc. SPIE* **9323**, 93230I–93230I–6 (2015).
[20] Franz, A., Haidegger, T., Birkfellner, W., Cleary, K., Peters, T., and Maier-Hein, L., "Electromagnetic tracking in medicine; a review of technology, validation, and applications," *Medical Imaging, IEEE Transactions on* **33**, 1702–1725 (Aug 2014).
[21] März, K., Franz, A., Seitel, A., Winterstein, A., Bendl, R., Zelzer, S., Nolden, M., Meinzer, H.-P., and Maier-Hein, L., "Mitk-us: real-time ultrasound support within mitk," *International Journal of Computer Assisted Radiology and Surgery* **9**(3), 411–420 (2013).